Available online at www.sciencedirect.com
ScienceDirect
Journal of the European Ceramic Society 31 (2011) 1533–1540
www.elsevier.com/locate/jeurceramsoc

Transparent hydroxyapatite ceramics with nanograin structure prepared by high pressure spark plasma sintering at the minimized sintering temperature

Mirva Eriksson [a], Yi Liu [a], Jiangfeng Hu [a], Lian Gao [b], Mats Nygren [a], Zhijian Shen [a,*]

[a] *Department of Materials and Environmental Chemistry, Arrhenius Laboratory, Stockholm University, S-10691 Stockholm, Sweden*
[b] *State Key Lab of High Performance Ceramics and Superfine Microstructure, Shanghai Institute of Ceramics, Chinese Academy of Sciences, Shanghai 200050, China*

Received 24 November 2010; received in revised form 8 March 2011; accepted 14 March 2011
Available online 9 April 2011

Abstract

A hydrothermally processed bulky powder composed of loosely aggregated nano-sized rods was consolidated by spark plasma sintering. The use of a high pressure cell allows the application of pressure up to 500 MPa. It was found that applying of high pressure is beneficial for widening up the kinetic window for attaining dense HAp nanoceramics. The high transparency of HAp nanoceramics obtained in this study is ascribed to the high density and homogeneous nano-grained structure achieved besides the unique intrinsic optical properties of the HAp crystal itself, i.e. its low refractive index and very small birefringence. Achieving full densification at the minimized sintering temperature allows for the first time the preparation of transparent HAp nanoceramics with stoichiometric composition, i.e. avoiding the loss of structural water that commonly takes place during the conventional ways of sintering.

Keywords: Hydroxyapatite; Ceramic structure; Microstructure; Nanoparticle; Sintering

1. Introduction

Hydroxyapatite, having a composition of $Ca_{10}(PO_4)_6(OH)_2$, denoted as HAp below, is one most widely investigated bioceramic material. HAp ceramics are bioactive, i.e. they promote bone apposition and growth on their surface.[1,2] Dense HAp ceramics are hardly used in orthopaedic and dental clinic due to its intrinsic poor mechanical properties. HAp is instead used in the forms of porous granules, porous scaffolds, coatings or bioactive fillers in composites. Yet, efforts are continuously dedicated to the development of dense bulk HAp ceramics with tailored microstructures. The aims of these works are in part to improve the mechanical performances, but are mainly for the development of dense bulk HAp ceramics to be used as prototype materials in connection with studies of the interactions between bioceramics and proteins and/or cells on different length scales.[3] Such fundamental studies are essential for understanding the biomineralization processes that occurs in the vicinity of the implants and will validate critical materials parameters for future engineering work on hard tissues. In this regard, transparency and nanostructured feature constitute two important material parameters that will determine the possible application of confocal microscopy allowing direct observation of the bio-interfacial reactions with improved spatial and temporal resolution.[4,5]

Optical transparency is readily achievable in HAp ceramics despite HAp possess a non-cubic crystal symmetry. There are already a number of reports that deals with preparation of transparent HAp ceramics. However, quite a few of these can hardly be regarded as transparent, but rather as translucent, as they show a very low transparency. Thought it is not our intention to make a full survey of the literature on this topic, it is worthwhile to refer to the following pioneer studies that led to the development of optical transparent HAp bulk ceramics and their associated sintering techniques, namely, (i) pressure-less sintering (PLS) of filter-cakes by Jarcho et al.[6]; (ii) hot isostatic pressing (HIP) of filter-cakes by Uematsu et al.[7]; (iii) hydrothermal hot pressing of amorphous calcium phosphate by Iouku et al.[8] (iv) microwave sintering of cold isostatic pressed (CIP) pellets by Feng et al.[9]; and (v) spark plasma sintering (SPS) of dry powders by Ioku et al.[10] and Watanabe et al.,[11] respectively.

* Corresponding author.
E-mail address: shen@mmk.su.se (Z. Shen).

0955-2219/$ – see front matter © 2011 Elsevier Ltd. All rights reserved.
doi:10.1016/j.jeurceramsoc.2011.03.021

Through a wet-chemistry process green bodies free from particle aggregates can be formed and Jarcho et al. demonstrated for the first time that high optical translucence can be achieved in HAp ceramics by PLSing around 1000–1100 °C for 1 h.[6] Freshly prepared fine grained particles (∼20 nm) were used in their work, which underwent considerable grain growth during calcination and sintering. Grains of an average size of ∼150 and ∼280 nm were formed in dense ceramics sintered at 1000 and 1100 °C, respectively, indicating a growth factor *f* of ∼7.5 and ∼14, respectively. The growth factor *f* is defined as the average grain size in ceramics sintered at a specific temperature divided by the average size of the initial particles.

Following this work Uematsu et al. applied the HIP process to consolidate HAp filter-cakes prepared as above.[7] HAp ceramics were fully densified at 800 °C after 2 h when a hot isostatic pressure of 100 MPa was used. The reduction of the sintering temperature from 1000 to 800 °C yielded radically improved optical transparency and distinctly reduced grain size. Thus, a specimen with excellent transparency, almost as clear as glass, was shown in their report and the specimen was composed of grains with an average size of ∼100 nm. An *f*-factor of ∼5 was thus observed, implying that notable grain growth still occurred in spite of such a low sintering temperature. In the same communication, it was also mentioned that higher HIPing temperatures tended to reduce the optical transparency of specimens. When a dry powder with twice as large initial particle size was used the HIP resulted in opaque specimens, although the density and *f*-factor were similar (∼5) to the ones of the filter-cake derived specimens. These observations revealed the importance of homogeneity of the powder packing, nano-sized microstructure and high density, in achieving optical transparent HAp ceramics.

Feng et al.[9] used a similar wet-chemistry process as that described in Ref. 6 to produce a precipitate that was hydrothermally treated and dehydrated at 500 °C yielding a well-crystallized needle-formed powder with an average particle size of ∼100 nm × 25 nm (length × width), defined as nano-rods, see below. This powder was CIPed using a pressure of 350 MPa and yielding a green compact with relative high density (60%) that in turn was pressureless densified by a rapid microwave sintering process in air containing 50% relative humidity. The green body sintered at 1150 °C for 5 min resulted in a transparent HAp ceramic that was composed of grains with an average size of ∼0.25 μm, implying an *f*-factor of ∼5.

Spark plasma sintering (SPS) has also been applied to densify HAp powders. This technique gains benefits from the simultaneous application of high pressure and an efficient heating process. Ioku et al. have prepared transparent HAp ceramics having an average grain size of less than 500 nm by SPSing a hydrothermally treated fine grained powder at 900–1000 °C for 10 min under a uniaxial pressure of 60 MPa.[10] Watanabe et al. managed to fabricate transparent HAp ceramics that were highly textured by SPS. The spray-dried spherical HAp granules calcined at 800 °C for 3 h was sintered at 1200 °C for 10 min under a pressure of 50 MPa.[11] The specimen had a relative density of 99.7% and was composed of very coarse columnar grains (∼200 μm in width and ∼25 μm in length) that were aligned along their *c*-axis. Yet, the specimen obtained was transparent, with an optical transmittance larger than 70% for wavelengths exceeding 700 nm.

Thus, transparent HAp nanoceramics have so far only been successfully prepared by a comparably complicated process, i.e. by hot isostatic pressing of filter-cakes that are formed by a sophisticated wet-chemistry route. SPS and microwave sintering of dry powders have also resulted in transparent specimens but not in combination with a nano-grained microstructure.

Quite recently it was reported that HAp nanoceramics, not transparent, can be obtained by pressure-less sintering of green bodies composed of nanorods, with a length and thickness of 50 and 15 nm, respectively, and having a green body density of 55%.[12] The green bodies were PLSed to full density at 900 °C for 2 h and yielded a microstructure that was composed of equi-axed grains of an approximate size of 83 nm. Lowering the sintering temperature down to 850 °C resulted to even smaller grains (∼67 nm). A comparatively small *f*-factor of ∼3 and ∼2.5 for samples prepared 900 °C and 800 °C, respectively, was thus observed. The success was ascribed to the transformation of nanorods of high aspect ratio into equi-axed grains and the associated morphology-enhanced diffusion mechanism makes it possible to use lower sintering temperature. In fact, HAp nanorods of the size 84 nm × 33 nm (length × width) have previously been consolidated by SPS at 825 °C for 3 min using a pressure of 50 MPa[13] yielding translucent compacts having densities of ∼98.6% and grain sizes in the range of 130 nm × 98 nm (length × width), i.e. an *f*-factor of ∼2.

The aim of this study was to explore the possibility of producing transparent HAp nanograin ceramics by approaching the lowest possible sintering temperature for HAp in combination with high mechanical pressures. The low sintering temperatures should also be of benefit for the retention of the stoichiometry of the HAp during the sintering. The success in achieving highly transparent nano-sized HAp ceramics made it possible for us to characterize their transmittance in wavelength regions of UV–visible and IR.

2. Materials and methods

2.1. Starting powder

A lab-made non-calcined bulky powder prepared by a hydrothermal process was used; it is composed of loosely aggregated nano-rods with an average width and length of 18 and 45 nm, respectively, and a surface area 45 m^2/g. A detailed description of the preparation route has been given elsewhere.[13] It has been observed that the particle size and morphology of HAp are sensitive to two critical processing parameters, i.e. the hydrothermal and post-hydrothermal calcination temperatures.[12,13] The XRD pattern of this powder given in Fig. 7 below shows that the powder is well crystallized in agreement with the SEM and TEM pictures given in Fig. 1.

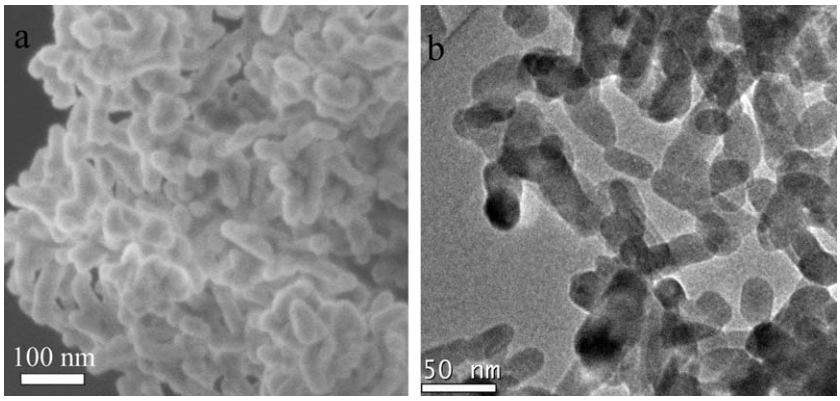

Fig. 1. The particle size and morphology of the starting powder as revealed by SEM (a) and TEM (b).

2.2. Sintering

The sintering was performed in vacuum in a SPS apparatus (Dr. Sinter 2050, SPS Syntex Inc., Kawasaki, Japan). The SPS unit is similar to a conventional hot press apparatus, i.e. the powder is loaded into a pressure die (see Fig. 2a) with an inner diameter of 12 mm, and the powder is submitted to a uniaxial pressure. In the SPS apparatus a pulsed direct current is lead through the sample holder, which usually is made of graphite. Thus the pressure die also serves as heating element. The sintering is normally performed in vacuum in a chamber that is water cooled. The direct current is regulated by pulses having a duration of 3.3 ms. The number of pulses per time unit can be varied but in this study we have used a pulse sequence of 12:2 which means that twelve pulses of DC current goes through the die/sample followed by two time periods (6.6 ms) of no current. The SPS process is described in more details in Ref. 14.

The maximum pressure the graphite die used in this study can withstand is ~150 MPa. A high pressure cell is used for pressures exceeding 150 MPa, see Fig. 2b. This cell is very similar to the one constructed by Anselmi-Tamburini et al.[15] and consists of two closely fitted graphite dies and the powder is loaded into inner one that has a diameter of 8 mm. The pressure is transferred from the punches associated to the outer graphite die through a set of load spreading disks to a pair of small internal punches, both made of binder-free tungsten carbide (WC) ceramic.

The temperature was measured by K-type thermocouple inserted 2 mm into the wall of the outer die when the high pressure cell was used while in all other experiments a pyrometer focused on the outer surface of the die was used to record the temperature. The shrinkage data were recorded during sintering and the data were corrected for the thermal expansion of the graphite parts.

It is well known that the sample is normally exposed to higher temperature than the recorded one in the SPS. The following experiments were performed in order to estimate this temperature gradient (ΔT); A solid piece of the dielectric $Na_{0.5}K_{0.5}NbO_3$ ceramic was inserted into the normal die with inner diameter of 12 mm and into the high pressure cell. The temperatures were measured with two pyrometers: one focused on the die surface and the other focused on the sample through a hole in the die. ΔT was measured at 800, 850, 900, 950 and 1000 °C after that stable ΔT – values were recorded. ΔT is found to be 40 °C at 800 °C for the normal die with diameter of 12 mm, while the high pressure cell experienced a ΔT of

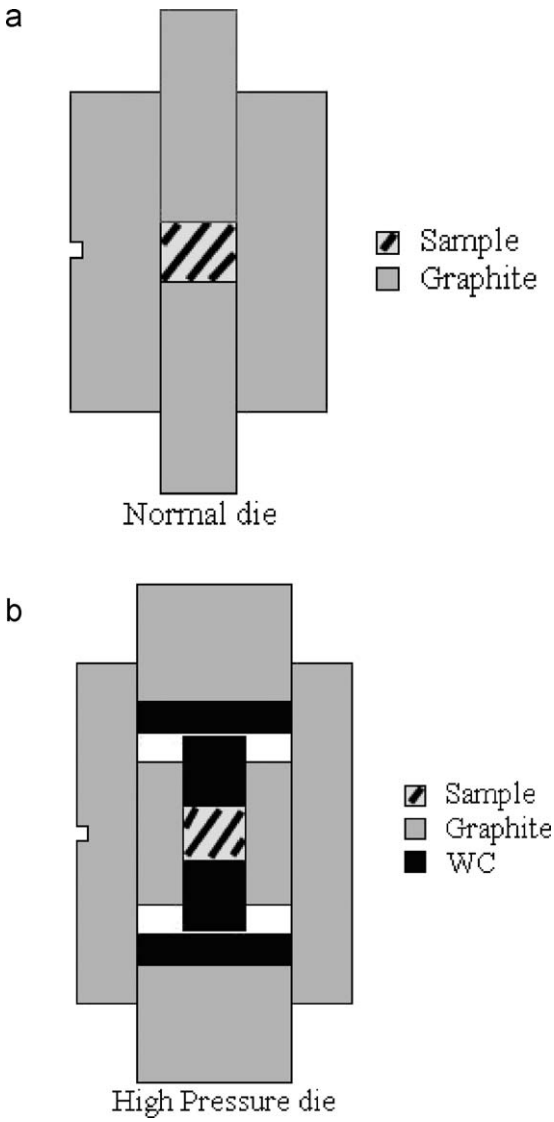

Fig. 2. Outline of a normal pressure die (a) and the high pressure one (b).

32 °C at the same temperature implying that in the temperature range of interest in this study the two experimental sets up used yields approximately the same ΔT.

One series of ceramics samples were sintered at 700, 750, 800, 850, 900, 950, and 1000 °C for 5 min using a pressure of 75 MPa (applied at room temperature) and a heating rate of 100 °C/min. In these experiments a normal die with inner diameter of 12 mm was used. Two samples were sintered with the heating rate of 50 °C/min up to 1000 °C without a holding time using pressures of 30 MPa and 75 MPa. The high pressure cell was used for sintering experiments at 700, 725, 750 °C. A heating rate of 50 °C/min was used and a holding time of 3 min. A pressure of 100 MPa was applied at room temperature that was increased at 150 °C to 200, 300, 400, or 500 MPa, respectively.

2.3. Phase and microstructure characterization

The densities of the SPS consolidated samples were measured according to Archimedes principle in water assuming that the theoretical density of HAp is 3.156 g cm^{-3}.[6]

The X-ray diffraction patterns (XRD) of the samples were recorded in a PANnalytical X'Pert instrument using Cu $K_{\alpha 1}$ radiation, and Rietveld refinement was used to calculate the cell parameters of HAp. The XRD patterns were also used to verify if decomposition of HAp have taken place during the sintering.

Microstructure characterization was carried out by transmission electron microscopy (TEM) and scanning electron microscopy (SEM) studies. The samples for TEM were prepared by ion slicing with an accelerating voltage of 5 kV, and investigated using the apparatus JEM-2000FXII (JEOL, Tokyo, Japan). A Field Emission Gun SEM (JSM-7000F, JEOL, Tokyo, Japan) was used for microstructure investigation of fracture surface as well of the polished surfaces. The samples were polished down to 4000 mesh with SiC sand paper and then with a suspension containing Al_2O_3 particles of ~300 nm. The samples were etched with 0.65 mg/ml HCl solution and coated with carbon prior to SEM investigation. The grain sizes were measured from the polished surfaces using linear intersection method with at least 300 grains and by measuring individual grains using image analyse program Image Tool (UTHSCSA).

2.4. Optical characterization

The absorption spectra in UV–visible region of the transparent and polished HAp samples were recorded with unpolarized light in the wavelength range 250–800 nm using a Zeiss MPM800 single-beam microscope-spectrometer. The transmittance in the IR region was measured from 400 to 4000 cm^{-1} with a Fourier transform infrared spectrometer (FTIR Varian 670-IR) equipped with a single-reflection Golden Gate ATR accessory with a diamond ATR element. The IR spectrum was used to estimate the loss of OH in connection with the sintering. The spectrums were scaled with the height of the absorption band of O–P–O bending modes of the PO_4^{3-} at 600 cm^{-1}.

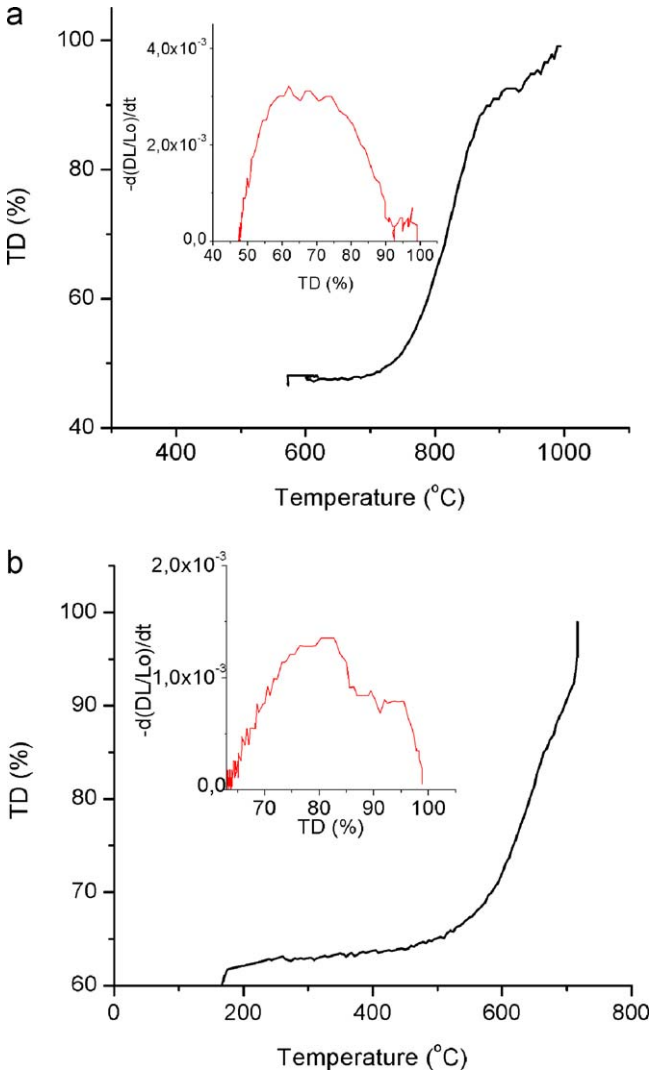

Fig. 3. Relative density as a function of temperature and densification rate as a function of relative density (inserted plot) recorded in real time during SPS processing of HAp using a normal die and a heating rate of 50 °C/min up to 1000 °C, a pressure of 75 MPa and no holding time (a) and the high pressure cell and a heating rate of 50 °C/min up to 700 °C, a pressure of 500 MPa and a holding time of 3 min (b).

3. Results and discussions

3.1. Minimizing sintering temperature by applying high pressures

The samples sintered in a normal die using 75 MPa did not achieve transparency but in the high pressure cell transparent samples could be sintered at 700 °C under 200 MPa. Transparent samples were also obtained when higher pressures were used but they frequently broke when they were removed from the cell possibly due to the release of internal stress. The densification and densification rate achieved under 75 and 500 MPa are plotted versus temperature and relative density in Fig. 3. The initial packing density increases from ~48% to over 60% when the pressure increases from 75 MPa to 500 MPa.

Table 1
The characteristic sintering kinetic parameters *vs* the SPS processing parameters.

SPS processing parameters[a]				Sintering kinetic parameters		
P	r_h (°C/min)	T_f (°C)	t (min)	T_d (°C)	$r_{d(\max)}$ (s^{-1})	RD_{max} (%) T (°C)
30 (N)	50	1000	0	780	0.0075	70 (840)
75 (N)	50	1000	0	750	0.0035	70 (820)
75 (N)	100	1000	5	740	0.006	70 (850)
100 (H)	50	750	3	634	0.002	72 (720)
200 (H)	50	725	3	610	0.0015	74 (650)
300 (H)	50	700	3	610	0.002	82 (650)
400 (H)	50	700	3	610	0.0015	84 (650)
500 (H)	50	700	3	570	0.0015	83 (650)

[a] SPS parameter: P = applied pressure in MPa, N = normal die, H = high pressure cell; r_h = heating rate; T_f = sintering temperature; t = holding time at T_f.

From this type of recorded sintering curves several important parameters that characterize the sintering kinetics can be extracted, namely, (i) the onset temperature of densification, T_d; (ii) the maximum densification rate achieved, $r_{d(\max)}$, defined as the maximum of $(1/\rho_{th}.d\rho/dt)$ with ρ_{th} being theoretical density of HAp; (iii) the relative density RD_{max} at which the $r_{d(\max)}$ appears. From Fig. 3 and from the data summarized in Table 1 it appears that applying a high pressure shifts the T_d to lower temperatures and the $r_{d(\max)}$ to slightly higher relative density.

This shift of the $r_{d(\max)}$ towards higher relative density implies an additional benefit gained by the application of high pressure, i.e. the time for the final sintering step and associated time for grain coarsening are reduced. The sintering period before reaching the maximum shrinkage can be empirically defined as the initial and intermediate stages of sintering, during which the densification is enhanced by the collapse of agglomerates, the rearrangement of particles by grain sliding, which are relatively fast.[16] Under a pressure of 500 MPa the maximum shrinkage is achieved at a relative density of ~81%, implying that only 19% of porosity needs to be removed by slower sintering mechanisms, e.g. by diffusional creep. It should be mentioned here that a $r_{d(\max)}$ value of the order of 10^{-2} to 10^{-3} s^{-1} is 1–2 orders of magnitude higher than what normally is achieved during conventional PLS.

The densification onset temperature, T_d, is to a great extent set by the characteristics of the powder, i.e. its chemical composition, phase constitution, particle size and aggregate status and as shown above on the sintering pressure used. In a previous dilatometer study it was revealed that the sintering of a hydrothermally synthesized HAp powder, similar to the present one, begins at around 670 °C.[9] This temperature can thus be regarded as the minimum temperature required to activate the interfacial diffusion of the HAp nanoparticles that is required for the densification. The application of high pressure reduced the T_d below this temperature but the final densification did not occur before the temperature for interfacial diffusion is approached as seen in Table 1.

As discussed above the hydrothermally synthesized HAp nanorods with an aspect ratio of ~3.4 experienced a distinct growth and morphology change to coarse uniaxial nanoparticles at 800 °C.[12] This observation indicates that the surface and interfacial diffusion of the HAp nanoparticles are sufficiently high already at 800 °C. It may also explain why this type of hydrothermally synthesized HAp nanoparticles can be fully densified by HIP at 800 °C[7] and by SPS at even lower temperature, 700 °C, when higher pressure is applied (≥200 MPa).

3.2. Temperature dependent of the grain growth

At the sintering temperatures the initial elongated nanoparticles were transformed into equiaxied nano-sized grains. The temperature-dependence of the densification and grain size in samples prepared at various temperatures are illustrated in Figs. 3 and 4. Two distinct evidences can be noticed, namely (i) densification occurs above T_d and increases with increasing temperature, see Fig. 3; and (ii) very limited grain growth occurs below a critical temperature, T_g, whereas above T_g grain growth takes place very rapidly within fully dense bodies. Such grain growth behaviour has previously been observed in connection with consolidating of various types of nanopowders by SPS.[17,18]

The temperature interval between T_d and T_g defines a *kinetic window* or *processing window* within which nanoceramics can be produced with controlled porosities. As shown in Fig. 4, this

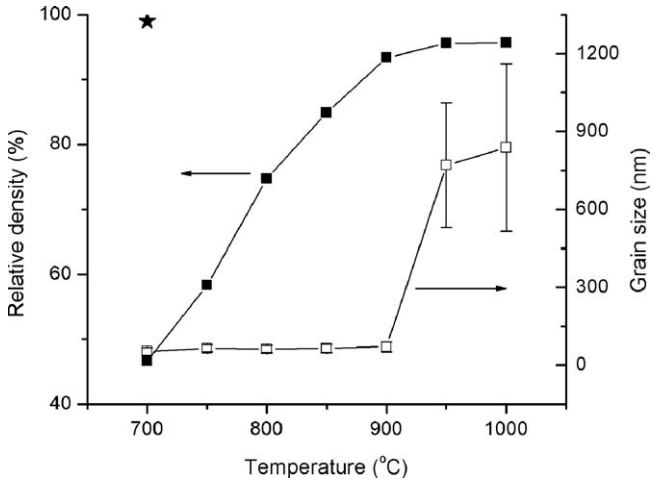

Fig. 4. Temperature-dependence of the densification and grain size. A normal die is used in these experiments and the sintering conditions used are: heating rate: 100 °C/min, holding time: 5 min, pressure 75 MPa. The star (100% TD, 700 °C) represents a transparent ceramic prepared in the high pressure cell using a pressure of 200 MPa and having an average grain size of 72 nm.

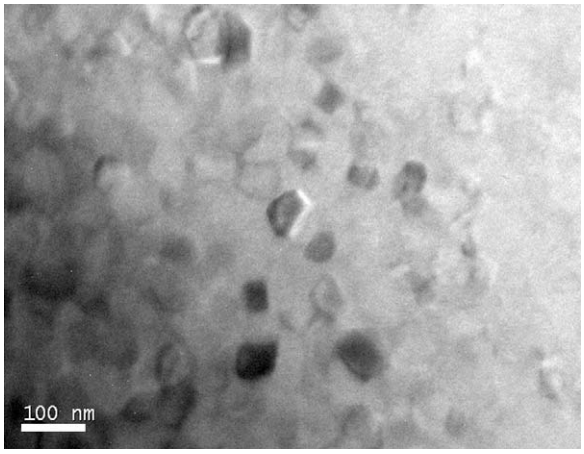

Fig. 5. A TEM micrograph of the transparent HAp ceramic sample consolidated at 700 °C for 3 min under 400 MPa.

kinetic window for preparing fully dense HAp nanoceramics can be widened by applying high pressures. The microstructure of a dense HAp ceramic specimen with average grain size of 64 nm is shown in Fig. 5.

The observed *f*-factors for SPSed samples are plotted versus the sintering temperature in Fig. 6 together with previously reported *f*-values for pressure-less, microwave sintered and HIPed specimens. It is obvious that the grain growth is suppressed by application of high pressures.

3.3. Phase purity and crystallinity of HAp

The XRD patterns of the HAp powder and of the bulk specimens consolidated at 700 °C and at 900 °C for 5 min under 75 MPa are given in Fig. 7. As the recorded patterns of the compacts and the starting powder are identical and so are the cell parameters (see Table 2), it can be concluded that no decomposition had taken place during sintering.

However, it is well known that HAp loses water upon heat treatment and that the apatite structure can accommodate OH vacancies before it finally decompose into β-tricalcium phosphate (β-TCP) or to any other phosphates. In a previous study it has shown that the loss of water is negligible if the sintering temperature is below 800 °C,[18] implying that we expect that the HAp nanoceramics prepared below 800 °C have stoichiometric composition whereas the ones prepared above 800 °C may contain OH vacancies.

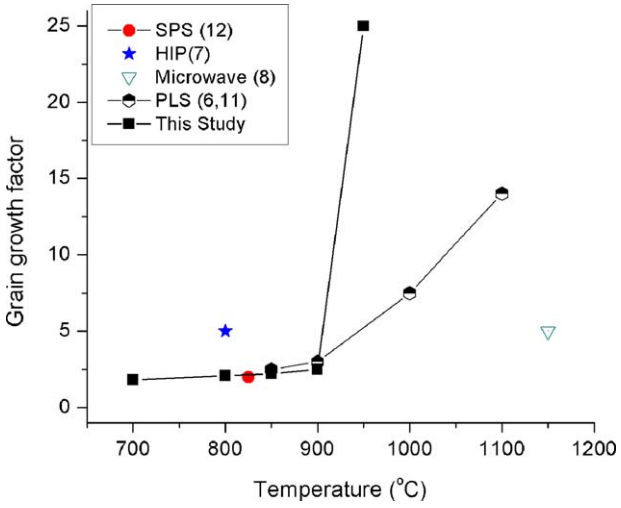

Fig. 6. The grain growth factor, *f*, plotted versus the sintering temperature.

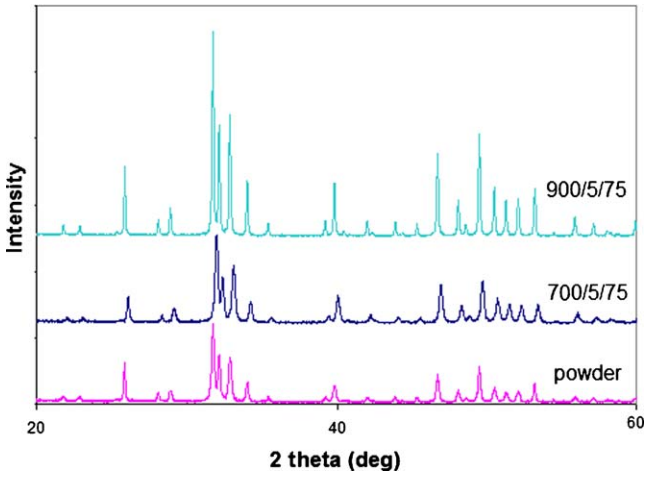

Fig. 7. The XRD patterns of the starting powder and of ceramics consolidated at 700 °C and 900 °C under 75 MPa for 5 min.

3.4. Optical properties of dense HAp nanoceramics

Clear and transparent HAp nanoceramics were prepared in the high pressure cell. The transmission spectrum in the UV–visible regime of a HAp ceramic having a thickness 0.7 mm is shown in Fig. 8. A transmittance of 70% is observed for wavelengths exceeding 450 nm. Besides one intensive absorption edge in the UV part (see below) no other absorption bands were noticed, indicating the HAp nanoceramics are transparent in the entire visible light regime.

The unique intrinsic optical properties of the HAp crystal,[19] i.e. its optical transparency, low refractive index, $n\omega = 1.651$, $n\varepsilon = 1.644$, and a very small birefringence, $\delta = 0.007$, suggest

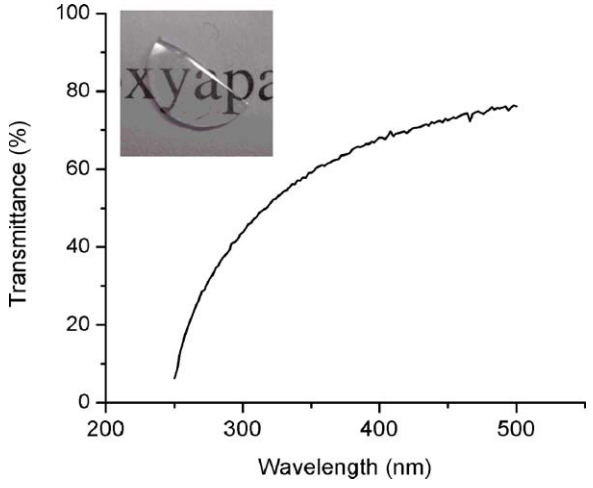

Fig. 8. UV–visible transmission spectrum recorded on a 0.7 mm thick HAp nanoceramic specimen consolidated at 700 °C for 3 min under 300 MPa.

Table 2
The unit cell parameters of HAp crystals in initial powder and in consolidated nanoceramics obtained by Rietveld refinement.

Material	SPS processing parameters[a]				Unit cell parameters	
	P	r_h (°C/min)	T_f (°C)	t (min)	a, b (Å)	c (Å)
Powder					9.418(1)	6.883(5)
Ceramic	75	100	700	5	9.427(3)	6.889(2)
Ceramic	75	100	900	5	9.422(1)	6.881(5)

[a] SPS parameter: P = applied pressure in MPa; r_h = heating rate; T_f = sintering temperature, t = holding time at T_f.

that it is possible to prepare transparent HAp ceramics. The loss of optical transparency of polycrystalline HAp is mainly due to the two microstructural factors, i.e. light scattering by pores and grain boundaries.[20] Like most of transparent oxide materials HAp nanoceramics exhibit an absorption edge in the UV-B regime (290–320 nm). This kind of UV-blocking property can be ascribed to the presence of defects (pores), most probably accommodated in grain boundaries. This UV-blocking in the UV-B regime is illustrated in Fig. 9 where the recorded spectra for two samples, one consolidated at 700 °C for 3 min under 500 MPa and the other one at 725 °C for 3 min under 200 MPa, are given. The relative density and average grain size of the former one is 99.9% and 84 nm, respectively, and corresponding data for the latter one are 99.3% and 86 nm, respectively. Thus a slight decrease of the density implies an increase of light scattering by small pores and a slight increase of the wavelength of the scattered light as seen in Fig. 9.

A part of the absorption spectrum of a HAp nanoceramic sample in the infrared region is given in Fig. 10a. The absorptions at 460–630 cm^{-1} are O–P–O bending modes of the PO_4^{3-} and at 962–1135 cm^{-1} are asymmetric P–O stretching modes of the PO_4^{-3}. The peak at 600 cm^{-1} is used to normalise the spectra recorded for HAp nanoceramics consolidated at different temperatures. The absorption peak at 3570 cm^{-1} is caused by OH^- stretching and the intensity of this peak can be used to estimate the concentration of OH vacancies. The normalised peaks O–H stretching peak recorded for specimens sintered at 700, 800 and 1000 °C are given in Fig. 10b. It should be noted that the spectra of the sample prepared at 700 °C and the starting powder was almost identical suggesting that the OH content of these samples is similar while OH-content of samples sintered at 800 °C or above is lower in agreement with findings discussed above. The IR-spectra of the starting powder and of the sintered compacts contained peaks that could be ascribed to carbonate, indicating that the sintering temperatures and the holding times used in this study are too low and too short for removing the

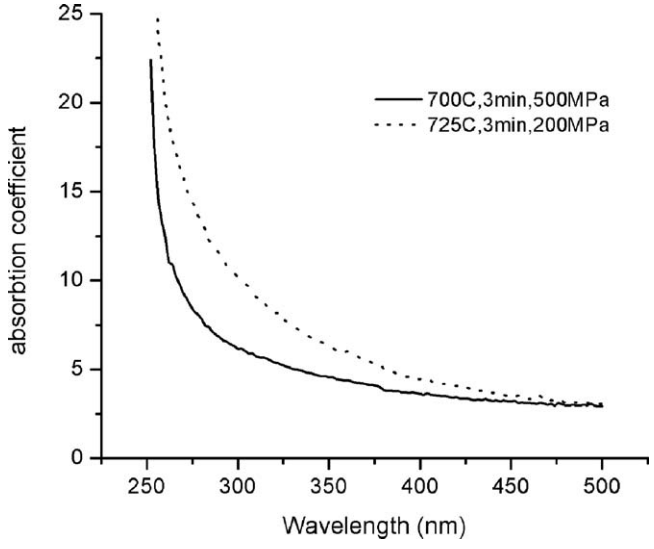

Fig. 9. The absorption edges of two HAp nanoceramic samples with almost same grain size but slightly different relative densities consolidated at 700 °C for 3 min under 500 MPa and at 725 °C for 3 under 200 MPa, respectively.

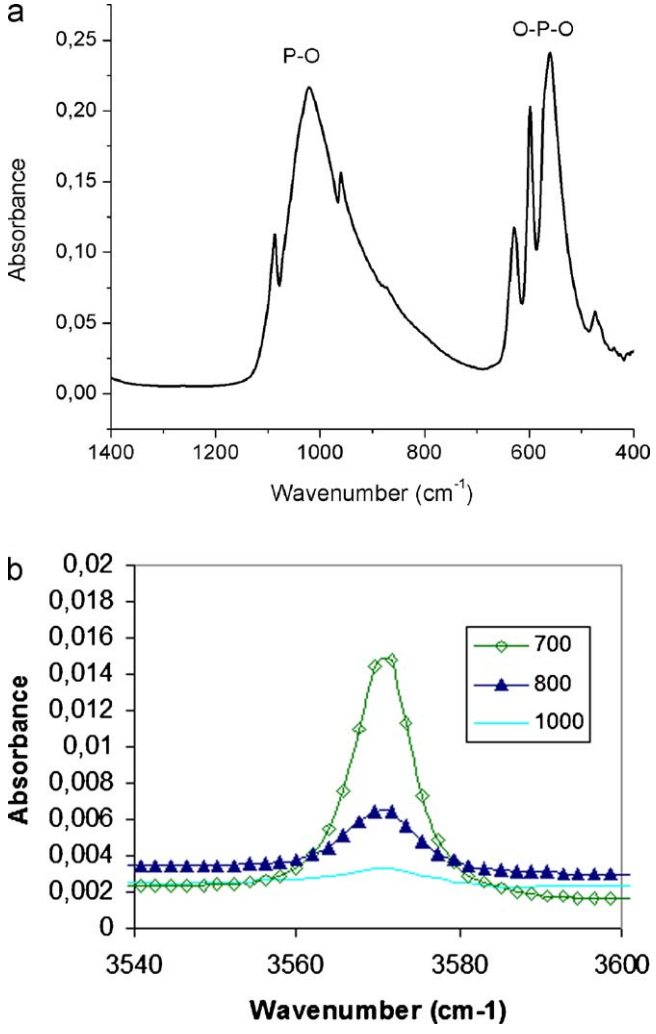

Fig. 10. IR absorption spectra of the PO_4^{-3} bands of a HAp ceramic sample consolidated at 700 °C for 3 min under 300 MPa (a), and the variation of the peak height of the OH band with the sintering temperature (b).

carbonate. As the pressure die is made of graphite it is not possible to exclude that some minor amounts of carbonate is formed during the sintering.

4. Conclusion

Applying high pressure is found to be beneficial for widen up the *kinetic window* towards lower temperatures for obtaining dense HAp nanoceramics. Reducing the sintering temperature makes it possible to prepare fully dense transparent HAp nanoceramics with stoichiometric composition. Applying a high pressure at reduced sintering temperatures is helpful for reducing porosity and pore size. Applying a slightly higher sintering temperature below T_g may not substantially alter the average grain size but it may have a tremendous influence on optical transparency due to formation of larger pores. The *kinetic window* for preparing transparent ceramics may thus be even smaller than the *kinetic window* that allows preparation of fully dense nanoceramic specimens. The high transparency of HAp nanoceramics obtained in this study is ascribed to the high density and homogeneous nano-grained structure achieved. The transparent HAp nanoceramics are suitable for direct observation of the bio-interfacial reactions with improved spatial and temporal resolution by confocal microscopy.

Acknowledgements

We would like to thank prof. Ulf Hålenius from the Swedish Museum of Natural Science for the help with the UV-vis measurements. This work was supported by the Swedish Governmental Agency for Innovation Systems (Vinnova) and the Swedish Research Council (VR) through the Berzelii Center EXSELENT on porous materials. The support of the Knut and Alice Wallenberg foundation for the purchase of electron microscopes used in this study is gratefully acknowledged. We would like to acknowledge VR for supporting the international collaboration involved in this work through its link programme.

References

1. Roy DM, Linnehan SK. Hydroxyapatite formed from coral skeletal carbonate by hydrothermal exchange. *Nature* 1974;**247**:220–2.
2. Kokubo T, Takadam H. How useful is SBF in predicting in vivo bone bioactivity? *Biomaterials* 2006;**27**(15):2907–15.
3. Webster TJ, Ergun C, Doremus RH, Siegel RW, Bizios R. Enhanced functions of osteoblasts on nanophase ceramics. *Biomaterials* 2000;**21**(7):1803–10.
4. Boyde A, Wolfe LA, Maly M, Jones SJ. Vital confocal microscopy in bone. *Scanning* 1995;**17**:72–85.
5. Kotobuki N, Ioku K, Kawagoe D, Fujimori H, Goto S, Ohgushi H. Observation of osteogenic differentiation cascade of living mesenchymal stem cells on transparent hydroxyapatite ceramics. *Biomaterials* 2005;**26**:779–85.
6. Jarcho M, Bolen CH, Thomas MB, Bobick I, Kay JF, Doremus RH. Hydroxyapatite synthesis and characterization in dense polycrystalline form. *J Mater Sci* 1976;**11**:2027–35.
7. Uematsu K, Takagi M, Honda T, Uchida N, Saito K. Transparent hydroxyapatite prepared by hot isostatic pressing of filter cake. *J Am Ceram Soc* 1989;**72**:1476–8.
8. Iouku K, Yamamoto K, Yanagisawa K, Yamasaki N. Low temperature sintering of hydroxyapatite by hydrothermal hot-pressing. *Phosphorus Res Bull* 1994;**4**:68–70.
9. Fang Y, Agrawal DK, Roy DM, Roy R. Fabrication of transparent hydroxyapatite ceramics by ambient-pressure sintering. *Mater Lett* 1995;**23**:147–51.
10. Ioku K, Kawagoe D, Toya H, Fujimori H, Goto S, Ishida K, et al. OH-designed transparent apatite ceramics prepared by spark plasma sintering. *Trans Mater Res Soc Jpn* 2002;**27**:447–9.
11. Watanabe Y, Ikoma T, Monkawa A, Suetsugu Y, Yamada H, Tanaka J, et al. Fabrication of transparent hydroxyapatite sintered body with high crystal orientation by pulse electric current sintering. *J Am Ceram Soc* 2005;**88**(1):243–5.
12. Wang J, Shaw L. Morphology-enhanced low temperature sintering of nanocrystalline hydroxyapatite. *Adv Mater* 2007;**19**:2364–9.
13. Guo X, Xiao P, Liu J, Shen Z. Fabrication of nanostructured hydroxyapatite via hydrothermal synthesis and spark plasma sintering. *J Am Ceram Soc* 2005;**88**(4):1026–9.
14. Shen ZJ, Johnsson M, Zhao Z, Nygren M. Spark plasma sintering of alumina. *J Am Ceram Soc* 2002;**85**(8):1921–7.
15. Anselmi-Tamburini U, Garay JE, Munir ZA. Fast low-temperature consolidation of bulk nanometric ceramic materials. *Scripta Mater* 2006;**54**:823–8.
16. Shen z, Nygren M. Microstructural prototyping of ceramics by kinetic engineering: applications of spark plasma sintering. *Chem Rec* 2005;**5**:173–84.
17. Shen Z, Peng H, Liu J, Nygren M. Conversion from nano- to micron-sized structures: experimental observations. *J Eur Ceram Soc* 2004;**24**:3447–52.
18. Fujimori H, Toya H, Ioku K, Goto S, Yoshimura M. In situ observation of defects in hydroxyapatite up to 1200 °C by ultraviolet Raman spectroscopy. *Chem Phys Lett* 2000;**325**:383–8.
19. Phillips WR, Griffen DT. In: Woodford AO, editor. *Optical mineralogy*. San Francisco: W.H. Freeman and Company; 1981. p. 81–4.
20. Krell A, Klimke J, Hutzler T. Transparent compact ceramics: inherent physical issues. *Opt Mater* 2009;**31**:1144–50.